

High Pressure Nitrogen-Infused Ultrastable Fuel Cell Catalyst for Oxygen Reduction Reaction

Eunjik Lee, Kurian A. Kuttiyiel,* Kyoung-Hee Kim, Jeongyun Jang, Hyo J. Lee, Jong M. Lee, Min H. Seo, Tae-Hyun Yang, Sung-Dae Yim, Jorge A. Vargas, Valeri Petkov, Kotaro Sasaki, Radoslav R. Adzic, and Gu-Gon Park*



Cite This: *ACS Catal.* 2021, 11, 5525–5531



Read Online

ACCESS |



Metrics & More



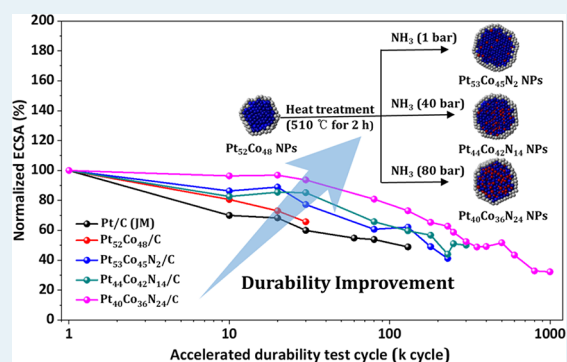
Article Recommendations



Supporting Information

ABSTRACT: The mass activity of a Pt-based catalyst can be sustained throughout the fuel cell vehicle life by optimizing its stability under the conditions of an oxygen reduction reaction (ORR) that drives the cells. Here, we demonstrate improvement in the stability of a readily available PtCo core–shell nanoparticle catalyst over 1 million cycles by maintaining its electrochemical surface area by regulating the amount of nitrogen doped into the nanoparticles. The high pressure nitrogen-infused PtCo/C catalyst exhibited a 2-fold increase in mass activity and a 5-fold increase in durability compared with commercial Pt/C, exhibiting a retention of 80% of the initial mass activity after 180 000 cycles and maintaining the core–shell structure even after 1 000 000 cycles of accelerated stress tests. Synchrotron studies coupled with pair distribution function analysis reveal that inducing a higher amount of nitrogen in core–shell nanoparticles increases the catalyst durability.

KEYWORDS: core–shell nanostructures, electrocatalyst, fuel cell, nitrogen doping, oxygen reduction



INTRODUCTION

Extensive practical applications of the commercial hydrogen fuel cell vehicle have been delayed because of the high cost and limited durability of the membrane electrode assembly (MEA).^{1–5} One of the main reasons for the high cost of the MEA is the large amount of Pt used to catalyze the oxygen reduction reaction (ORR) at the cathode of the proton exchange membrane (PEM) fuel cell. In the past decade, several studies investigated ORR electrocatalysts to reduce the cost of the MEA. One of the main strategies is to add modifiers to the Pt catalyst by changing the structure and morphology of the PtM (metal) alloy catalyst,^{6–11} while others include completely avoiding Pt usage by using various nonprecious M–N–C moiety catalysts.^{12–16} Although the addition of modifiers can drastically increase catalytic performance, it cannot be sustained for prolonged periods, which is a major factor impeding commercialization.^{17–19}

To date, carbon-supported PtCo alloy nanoparticles have emerged as the best alternative to Pt/C; original equipment manufacturers are already using them in first-generation hydrogen fuel cell vehicles.^{20,21} For better Pt utilization efficiency throughout the fuel cell lifetime, an ideal catalyst should be able to maintain its electrochemical surface area (ECSA).^{22–24} Although earlier studies have corroborated nitrogen's role in stabilizing the catalyst,^{25,26} high pressures doping of nitrogen in a controlled environment on industrial

scale core–shell nanoparticles was not achieved. Thus, in this study, to obtain a highly stable and active ORR catalyst, a high-pressure nitrating reactor that can infuse a controlled number of nitrogen (N) atoms into the alloy nanoparticles was developed. Varying the ratio of N atoms in the PtCo/C core–shell nanoparticles can significantly affect the morphology of the nanoparticles and simultaneously increase their stability without impacting the activity. Herein, we report the preparation of N-stabilized PtCo core–shell nanoparticles with ultrastable configurations; the result is a highly durable ORR catalyst that can withstand up to 1 000 000 cycles in accelerated stress tests (ASTs), enabling rapid commercialization of fuel cell vehicles. To the best of our knowledge, thus far, no catalysts have been reported that can last 1 million cycles. The best configuration (Pt₄₀Co₃₆N₂₄/C) retained 93% of its ECSA, while its initial half-wave potential decreased by only 6 mV after 30 000 cycles. This confirms that the proposed configuration is a suitable alternative to the commercial Pt/C

Received: January 27, 2021

Revised: March 22, 2021



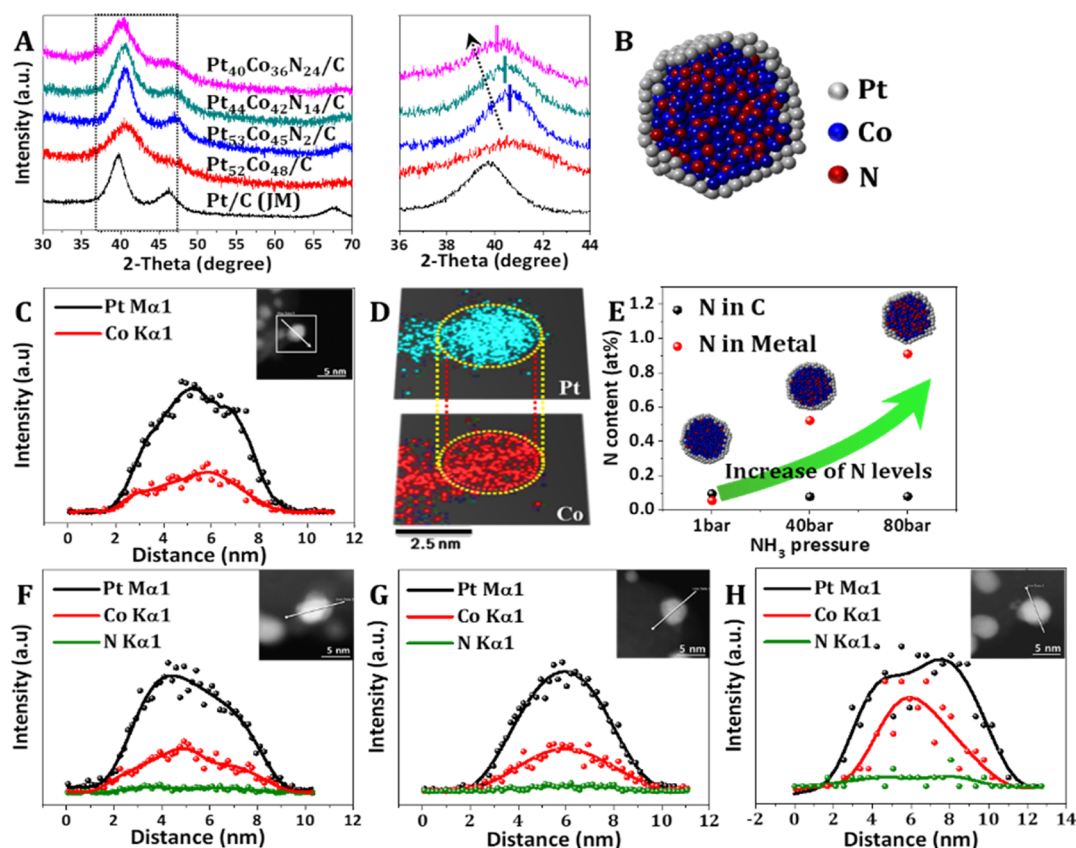


Figure 1. Structure and chemical composition characterization of PtCoN nanoparticles. (A) In-house XRD patterns of N–PtCo/C nanoparticles together with the magnified profiles of the first XRD peak. (B) Cross section of a 3D model of a $\text{Pt}_{40}\text{Co}_{36}\text{N}_{24}/\text{C}$ nanoparticle. (C, D) EDS line scan and corresponding EDS maps of a $\text{Pt}_{52}\text{Co}_{48}/\text{C}$ nanoparticle. (E) N content of nanoparticles determined from EA analysis. (F–H) EDS line scans of $\text{Pt}_{53}\text{Co}_{45}\text{N}_2/\text{C}$, $\text{Pt}_{44}\text{Co}_{42}\text{N}_{14}/\text{C}$, and $\text{Pt}_{40}\text{Co}_{36}\text{N}_{24}/\text{C}$. The insets show the corresponding STEM images.

Table 1. Physicochemical Properties of Catalyst Based on X-ray Diffraction, Tunneling Electron Microscopy, Elemental Analyzer Studies, and Electrochemical Data^a

sample	particle size (nm)	N content metal (%)	molar ratio Co/N	lattice const (nm)	Pt–Pt dist (nm)	ECSA ($\text{m}^2/\text{g}_{\text{Pt}}$)	SA ($\mu\text{A}/\text{cm}^2_{\text{Pt}}$)	MA ($\text{A}/\text{mg}_{\text{Pt}}$)
Pt/C (JM)	3.1			0.3930	0.2780	54.0	418.6	0.226
$\text{Pt}_{52}\text{Co}_{48}/\text{C}$	2.3			0.3837	0.2713	81.9	600.6	0.492
$\text{Pt}_{53}\text{Co}_{45}\text{N}_2/\text{C}$	4.2	0.05	23.63	0.3843	0.2717	65.5	889.6	0.572
$\text{Pt}_{44}\text{Co}_{42}\text{N}_{14}/\text{C}$	3.9	0.52	3.0	0.3856	0.2726	67.2	716.5	0.482
$\text{Pt}_{40}\text{Co}_{36}\text{N}_{24}/\text{C}$	3.7	0.91	1.56	0.3880	0.2743	53.7	847.6	0.455

^aSA, specific activity; MA, mass activity.

catalyst, whose ECSA deteriorated by 40% under similar conditions.

RESULTS AND DISCUSSION

Carbon-supported PtCo core–shell nanoparticles were prepared by reducing platinum acetylacetonate [$\text{Pt}(\text{acac})_2$] and cobalt acetylacetonate [$\text{Co}(\text{acac})_2$] via ultrasound-assisted polyol synthesis. Transmission electron microscopy (TEM) analysis showed that the as-synthesized PtCo nanoparticles exhibited a core–shell structure with an average particle size of ~ 2.3 nm (Figure S1). Scanning TEM (STEM) and energy-dispersive X-ray spectroscopy (EDS) confirmed the core–shell structure with 1–2 Pt monolayers on the Co-rich core (Figure 1B–D). The PtCo core–shell nanoparticles were annealed in an argon/ammonia mixture (N_2/NH_3 : 5/95) at 510 °C in three pressurized environments (1, 40, and 80 bar). The nanoparticles maintained their core–shell structures and

exhibited an increase in the particle size and a change in composition (Figure 1F–H). As shown in Figure 1E, higher pressure increases the N content in the nanoparticles but ultimately decreases the particle size. On the basis of the N content in the nanoparticles, the molar ratio changes drastically; the resultant nanoparticles are denoted as $\text{Pt}_{52}\text{Co}_{48}/\text{C}$, $\text{Pt}_{53}\text{Co}_{45}\text{N}_2/\text{C}$, $\text{Pt}_{44}\text{Co}_{42}\text{N}_{14}/\text{C}$, and $\text{Pt}_{40}\text{Co}_{36}\text{N}_{24}/\text{C}$ (Table 1). For all samples, in-house X-ray diffraction (XRD) patterns exhibit the typical face-centered-cubic (fcc) structure, with no phase segregation, corresponding to Pt and its alloys with transition metals (JCPDS, No. 87-0646) (Figure 1A). The position of the (111) peak of PtCo/C shifts to a higher angle compared with that of Pt/C, indicating that Co atoms with relatively smaller atomic sizes are incorporated into the Pt lattice, causing compressive strain. Interestingly, the nitriding pressure directly affects the full width at half-maximum (fwhm) and position of the (111)

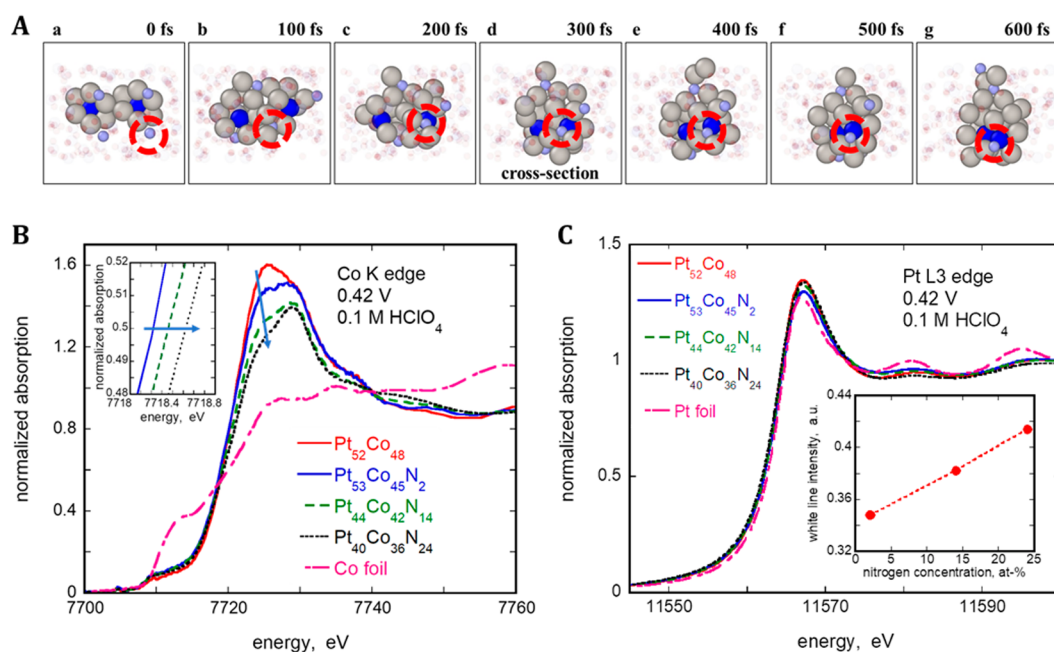


Figure 2. Molecular dynamics simulations and XANES analysis of PtCoN nanoparticles. (A) Ab initio molecular dynamics results showing the agglomeration of two $\text{Pt}_{12}\text{Co}_1$ particles in an NH_3 environment (e.g., 28.7 bar at 783 K). (B) In situ Co K edge XANES spectra of PtCo/C and N-PtCo/C catalysts measured in 0.1 M HClO_4 at 0.42 V. The inset shows the half-step energy values (at 0.5 of the normalized absorption in the XANES spectra) of N-PtCo/C catalysts. (C) In situ Pt L₃ edge XANES spectra of PtCo/C and N-PtCo/C catalysts measured in 0.1 M HClO_4 at a potential of 0.42 V. The inset shows the intensity of white lines of the XANES spectra plotted as a function of N concentration.

peak. In particular, the fwhm increases and the (111) peak position gradually shifts to a lower angle with an increase in the nitriding pressure. This suggests that the nitriding pressure changes the atomic structure of the catalyst particles while relaxing the lattice mismatch between Pt skin and cobalt nitride core (Table 1). Furthermore, X-ray photoelectron spectroscopy (XPS) studies indicate that, compared with metallic Pt, the Pt 4f peak in all samples shifts to a lower binding energy (BE), likely owing to the charge transfer from Co to Pt (Figure S2). Additionally, no peaks (~ 399.8 eV) for imides/lactams/amides are observed, indicating that most N in the samples exists in the form of nitrides.

To gain further insights about how the as-synthesized PtCo core-shell nanoparticles maintain their structures while incorporating N atoms, we carried out ab initio molecular dynamics (AIMD) studies to simulate the formation of the CoN nanophase in the nanoparticle core. Before the conduction of AIMD, the NH_3 molecules were packed into a unit cell with cuboctahedral PtCo nanoparticles under pressures of 1, 10, and 45 bar by use of the COMPASSII force field.^{27–29} We considered the entropic effect to identify the continuous reaction process incorporated at a finite temperature of 783 K. In the case of a single PtCo nanoparticle, it is found that N atoms from the NH_3 molecules cannot penetrate the Co core even at a high pressure of NH_3 , as shown in Figure S3 and Movie S1. Therefore, we tested the case of formation of PtCoN core-shell nanoparticles through a particle growth process involving the agglomeration of the preformed PtCo fragments into nitride cores that are consequently covered by a Pt shell. The results shown in Figure 2A indicate that this is the likely mechanism of the particle size increasing from ~ 2.3 nm for pure PtCo nanoparticles to ~ 4.2 nm for $\text{Pt}_{53}\text{Co}_{45}\text{N}_2/\text{C}$ (Table 1). Interestingly, AIMD studies are appreciably consistent with

the observation that two $\text{Pt}_{12}\text{Co}_1$ nanoparticles at 10 bar of NH_3 (e.g., 28.7 bar at 783 K) can spontaneously merge without any considerable activation barrier.

The simulations indicate the formation of irregular particles with a compressed Pt–Pt distance depending on the location of nearby N atoms, as revealed by the atomic pair distribution function (PDF) analysis and the reverse Monte Carlo modeling (discussed below), thereby increasing the number of N atoms that exist near the Pt sublayer.

In situ Co K edge X-ray absorption near-edge structure (XANES) spectra of $\text{Pt}_{52}\text{Co}_{48}/\text{C}$, $\text{Pt}_{53}\text{Co}_{45}\text{N}_2/\text{C}$, $\text{Pt}_{44}\text{Co}_{42}\text{N}_{14}/\text{C}$, and $\text{Pt}_{40}\text{Co}_{36}\text{N}_{24}/\text{C}$ nanoparticles (Figure 2B) were obtained in 0.1 M HClO_4 at a potential of 0.42 V. As the N concentration increases, the peak intensity at 7724 eV starts decreasing; the highest peak at 7727 eV is observed at a N concentration of >14 at%. This change can be ascribed to a change in the electronic structures of Co due to N doping. As shown in Figure S7, the XANES spectra of CoO (Co^{2+}) and Co_3O_4 ($\text{Co}^{2.67+}$) exhibit the highest peaks at 7725 and 7729 eV, respectively; meanwhile, the highest peak for $\text{Pt}_{40}\text{Co}_{36}\text{N}_{24}/\text{C}$ lies between them. Thus, the N doping of PtCo catalysts alters the electronic state of Co, resulting in an increase in the oxidation state. The increase in the oxidation state with an increase in the N content is also supported by the data shown in the inset of Figure 2B; half-step energy values (at 0.5 of the normalized absorption in the XANES spectra) increase with an increase in the N concentration. Figure 2C shows the in situ Pt L₃ edge XANES spectra of the PtCo/C and N-PtCo/C catalysts measured in 0.1 M HClO_4 at a potential of 0.42 V. The intensities of the white lines (first peaks in XANES data) change with the variation in the N content in the N-PtCo/C catalysts. As shown in the inset of Figure 2C, the intensity increases with increase in N concentration; it is higher than that of a Pt foil but lower than that of the PtCo/C catalyst. The

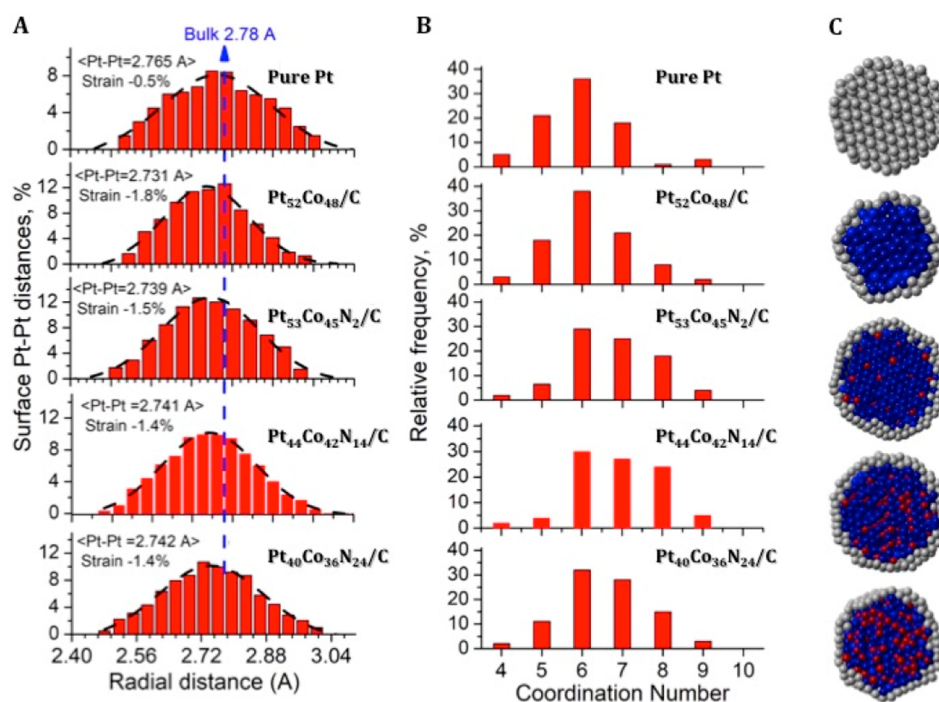


Figure 3. Results from synchrotron XRD experiments coupled to atomic PDF analysis and 3D modeling. (A) Surface Pt–Pt distances and (B) coordination numbers in PtCo core–shell particles extracted from (C) 3D models refined against experimental atomic PDFs. Pt, Co, and N atoms are shown in gray, blue, and red, respectively.

change in white line intensity is related to the d-band structure in Pt. It is well-known that higher intensities correspond to an increase in d-band vacancy;^{30–32} that in turn lowers the adsorption of the intermediate molecules (such as OOH and OH) on the Pt surface.^{33,34} Thus, N doping can weaken the interaction of the Pt surface with oxygen, compared with that of bulk Pt. However, the effect is not as strong as that for the PtCo/C catalyst as the white line intensity for the N–PtCo/C catalysts is lower than that of PtCo/C and varies with the N content. The XANES data suggest that N doping in N–PtCo/C alters the electronic states of Co and Pt, resulting in moderate adsorption strength of oxygen on the Pt surface.

To comprehensively understand the particle structure, high-energy synchrotron XRD experiments coupled with atomic PDF analysis were carried out. Experimental PDFs (Figure S8) were fit with 3D models for the nanoparticles using classical molecular dynamics (MD) simulations and were further refined against the experimental PDF data by employing reverse Monte Carlo modeling. Cross sections of the models emphasizing the core–shell characteristics of the particles are shown in Figure 3. The models exhibit a distorted fcc-type structure and reproduce the experimental data in exceedingly good detail (Figure S8). The bonding distances between the surface Pt atoms and surface Pt coordination numbers extracted from the models are also shown in Figure 3. As observed, PtCo core–shell particles exhibit large structural distortions (~1.8%). The surface Pt–Pt distance in Pt₅₃Co₄₅N₂ is 2.739 Å, which is approximately 1.5% shorter than the surface Pt–Pt distances in bulk Pt (2.765 Å). Furthermore, the surface Pt–Pt distance in PtCo is 2.731 Å, indicating 0.3% more strain compared with the strain observed in the Pt₅₃Co₄₅N₂ particles. This indicates that N relaxes the compressive stress in PtCo core–shell particles. Moreover, the average surface Pt coordination number for the particles

with CoN cores increases and becomes more evenly distributed than in the case of pure Pt particles; that is, the surfaces of N-treated particles appear less rough (fewer undercoordinated sharp edges and corners), which can affect the binding strength of oxygen molecules to the particle surface and accelerate the ORR kinetics. As expected, the N-treated particles show an increased number of N atoms located near the Pt shell, which explains the increased stability of the nanoparticles compared with those of pure Pt and PtCo particles.

The electrochemical performances of all the catalysts were compared using cyclic voltammetry (CV) curves (Figure S4). The incorporation of Co into the Pt nanoparticles increases the ECSAs of the catalysts, while that of N into the PtCo nanoparticles decreases their ECSAs (Figure 4A). A slightly different trend was observed with respect to the specific and mass activities of the catalyst (Figure 4B). The PtCo/C catalyst with low nitrogen content shows the highest activity among the catalysts; however, an increase in N content does not drastically change its catalytic behavior. Our study was mainly focused on achieving structural stability of the catalyst. AST cycles at 0.6–0.95 V and 3 s hold were employed for each catalyst. All N-infused PtCo/C catalysts showed higher stability and activity compared with commercially available Pt/C and PtCo/C catalysts (Figure S5). The catalyst with the highest N amount (Pt₄₀Co₃₆N₂₄/C) retained 93% of its ECSA, with a decrease of only 6 mV in its initial half-wave potential after 30 000 cycles. To further investigate the structural integrity of all the catalysts, we cycled them until the ORR activity decreased to half its initial value. As observed in Figure 4C, most of the N-infused catalysts retained their structures up to 230 000 cycles; however, the catalyst with the highest amount of N (Pt₄₀Co₃₆N₂₄/C) retained its structural integrity until 1 000 000 cycles and lost just 44 mV from its initial half-

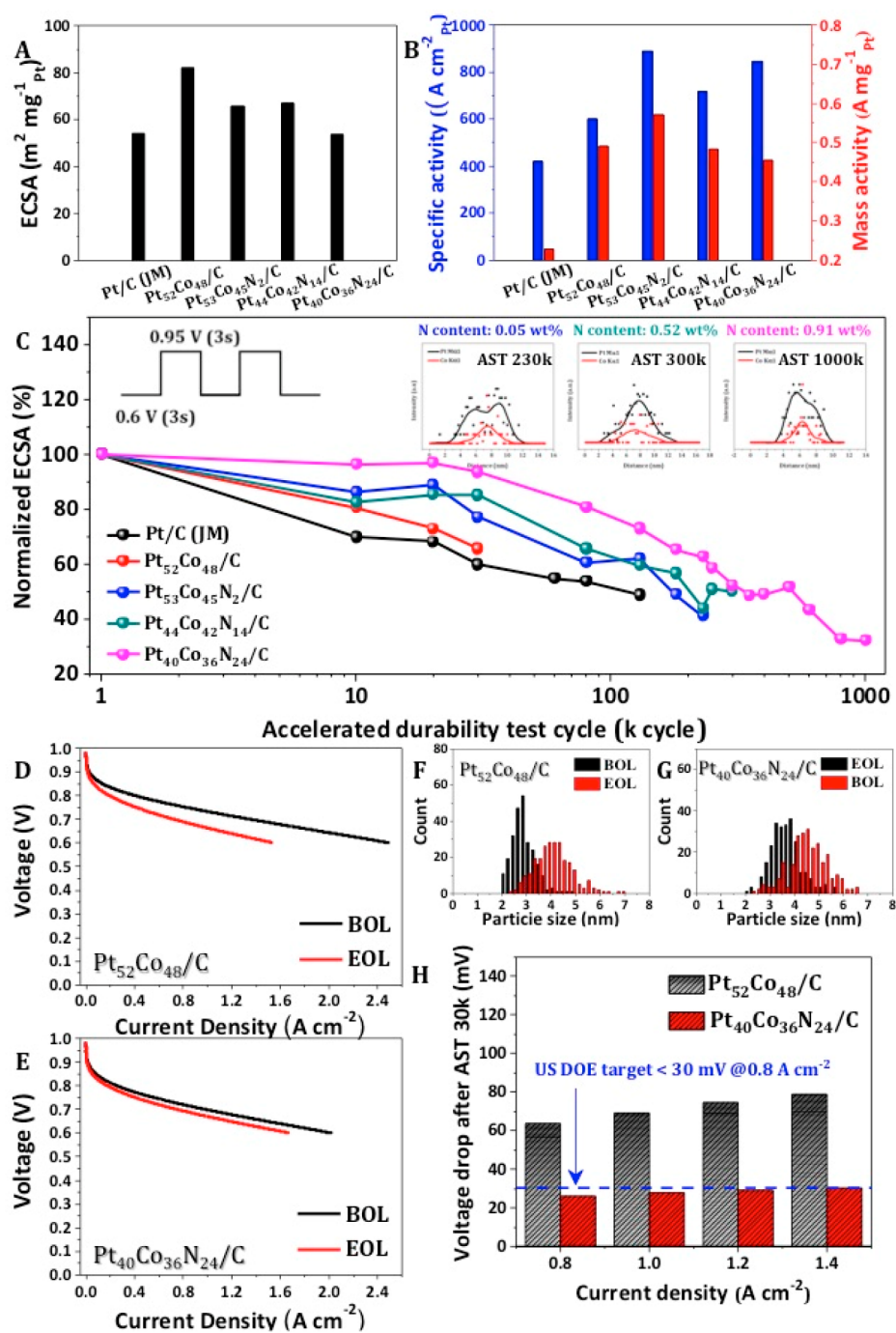


Figure 4. Electrochemical performance and durability of the catalysts. (A) Electrochemical surface area and (B) specific and mass activity at 0.9 V. (C) Normalized ECSA of the samples under ASTs. Inset shows EDS line scans of samples with varying N content (0.05–0.91 wt%) after ASTs. Fuel cell performance and durability of (D) $\text{Pt}_{52}\text{Co}_{48}/\text{C}$ and (E) $\text{Pt}_{40}\text{Co}_{36}\text{N}_{24}/\text{C}$ catalysts. (F, G) Nanoparticle size histograms of the catalysts before and after 30 000 ASTs. (H) Fuel cell comparisons of the voltage drop in catalysts after 30 000 ASTs at various current densities.

wave potential (Figure S6). Fuel cell (25 cm^2) performance tests with 0.1 mg cm^{-2} Pt content showed promising results (Figure 4D,E). The $\text{Pt}_{40}\text{Co}_{36}\text{N}_{24}/\text{C}$ catalyst achieves the U.S. Department of Energy durability target of a 30 mV voltage drop at 0.8 A cm^{-2} after 30 000 ASTs (Figure 4H). Moreover, considering the particle size growth after 30 000 ASTs, the PtCo nanoparticles grew by 41% from their initial average size (Figure 4F), whereas the N-infused PtCo nanoparticles grew by 21%, confirming that N plays a key role in impeding nanoparticle coarsening (Figure 4G). As previously reported,²⁶

DFT-based studies clearly support the higher ORR activities of nitride-stabilized Pt–metal electrocatalysts over Pt/C catalysts. Their volcano-like trends show that the interactions of Pt/C and PtCo/C with oxygen are significantly stronger and weaker, respectively, compared with those of PtCoN/C. The outstanding stability of high-pressure N-infused PtCoN/C catalysts can be easily explained on the basis of our recent DFT findings.¹⁰ The segregation effect of Pt facilitated by the higher N concentration in turn facilitates the diffusion of Pt atoms to the vacant sites of the outermost shell, preventing

dissolution. Evidently, these results demonstrate the enhanced catalytic stability of the Pt₄₀Co₃₆N₂₄/C catalyst over the other N-infused PtCo catalyst.

CONCLUSION

We exhibited that nanostructured core–shell materials with high contents of N in their cores can be engineered to sustain harsh and oxidative electrochemical environments during fuel cell operation. X-ray experiments and PDF analyses revealed that a high N content could protect the Co core against dissolution. The sustainment of 1 million cycles after harsh and corrosive ASTs without significant dissolution facilitates the potential industrial scale application of the catalysts. This strategy presents a promising approach to develop cheap and ultradurable core–shell catalysts using other 3d transition metal cores.

ASSOCIATED CONTENT

Supporting Information

The Supporting Information is available free of charge at <https://pubs.acs.org/doi/10.1021/acscatal.1c00395>.

AIMD simulations for PtCo nanoparticles, supplementary video clips (ZIP)

Materials and methods; TEM images, XPS data, AIMD simulations, CVs, LSVs, XANES spectra, PDFs (PDF)

AUTHOR INFORMATION

Corresponding Authors

Gu-Gon Park – Fuel Cell Laboratory, Korea Institute of Energy Research, Daejeon 34129, South Korea; orcid.org/0000-0002-4606-0661; Email: gugon@kier.re.kr

Kurian A. Kuttiyiel – Chemistry Department, Brookhaven National Laboratory, Upton, New York 11973, United States; Email: kurian@bnl.gov

Authors

Eunjik Lee – Fuel Cell Laboratory, Korea Institute of Energy Research, Daejeon 34129, South Korea

Kyoung-Hee Kim – Fuel Cell Laboratory, Korea Institute of Energy Research, Daejeon 34129, South Korea

Jeongyun Jang – Fuel Cell Laboratory, Korea Institute of Energy Research, Daejeon 34129, South Korea

Hyo J. Lee – Fuel Cell Laboratory, Korea Institute of Energy Research, Daejeon 34129, South Korea

Jong M. Lee – Fuel Cell Research & Demonstration Center, Korea Institute of Energy Research, Buan-gun, Jeollabuk-do 56332, South Korea

Min H. Seo – Fuel Cell Research & Demonstration Center, Korea Institute of Energy Research, Buan-gun, Jeollabuk-do 56332, South Korea; orcid.org/0000-0003-3910-4512

Tae-Hyun Yang – Fuel Cell Laboratory, Korea Institute of Energy Research, Daejeon 34129, South Korea

Sung-Dae Yim – Fuel Cell Laboratory, Korea Institute of Energy Research, Daejeon 34129, South Korea

Jorge A. Vargas – Department of Physics and Science of Advanced Materials Program, Central Michigan University, Mount Pleasant, Michigan 48859, United States; Unidad Académica de Física, Universidad Autónoma de Zacatecas, Zacatecas 98098, Mexico; orcid.org/0000-0002-9651-8183

Valeri Petkov – Department of Physics and Science of Advanced Materials Program, Central Michigan University,

Mount Pleasant, Michigan 48859, United States;

orcid.org/0000-0002-6392-7589

Kotaro Sasaki – Chemistry Department, Brookhaven National Laboratory, Upton, New York 11973, United States;

orcid.org/0000-0003-2474-8323

Radoslav R. Adzic – Chemistry Department, Brookhaven National Laboratory, Upton, New York 11973, United States

Complete contact information is available at:

<https://pubs.acs.org/10.1021/acscatal.1c00395>

Notes

The authors declare no competing financial interest.

ACKNOWLEDGMENTS

This study was supported by the Industrial Strategic Technology Development Program (NP2020-0040) funded by the Ministry of Trade, Industry & Energy (MOTIE, Korea) and the Korea Institute of Energy Research (C1-2417). The Fuel Cell Research & Demonstration Centre acknowledges support from a National Research Foundation of Korea Grant funded by the Korean Government [NRF-2017R1D1A1B04031539]. This article has also been authored by employees/guests of Brookhaven Science Associates, LLC, under Contract No. DE-SC0012704 with the U.S. Department of Energy. This research used resources of the ISS (8-ID) and QAS (7-BM) beamlines of the National Synchrotron Light Source II, which are U.S. DOE Office of Science Facilities, at Brookhaven National Laboratory, under Contract was also supported in part by “DE-SC0006877 grant”.

REFERENCES

- (1) Debe, M. K. Electrocatalyst approaches and challenges for automotive fuel cells. *Nature* **2012**, 486 (7401), 43–51.
- (2) Adzic, R. Platinum Monolayer Electrocatalysts: Tunable Activity, Stability, and Self-Healing Properties. *Electrocatalysis* **2012**, 3 (3–4), 163–169.
- (3) Ott, S.; Orfanidi, A.; Schmies, H.; Anke, B.; Nong, H. N.; Hübner, J.; Gernert, U.; Gliech, M.; Lerch, M.; Strasser, P. Ionomer distribution control in porous carbon-supported catalyst layers for high-power and low Pt-loaded proton exchange membrane fuel cells. *Nat. Mater.* **2020**, 19 (1), 77–85.
- (4) Stamenkovic, V. R.; Mun, B. S.; Arenz, M.; Mayrhofer, K. J. J.; Lucas, C. A.; Wang, G.; Ross, P. N.; Markovic, N. M. Trends in electrocatalysis on extended and nanoscale Pt-bimetallic alloy surfaces. *Nat. Mater.* **2007**, 6 (3), 241–247.
- (5) Wang, D. L.; Yu, Y. C.; Zhu, J.; Liu, S. F.; Muller, D. A.; Abruna, H. D. Morphology and Activity Tuning of Cu3Pt/C Ordered Intermetallic Nanoparticles by Selective Electrochemical Dealloying. *Nano Lett.* **2015**, 15 (2), 1343–1348.
- (6) Markovic, N. M.; Adzic, R. R.; Cahan, B. D.; Yeager, E. B. Structural Effects in Electrocatalysis - Oxygen Reduction on Platinum Low-Index Single-Crystal Surfaces in Perchloric-Acid Solutions. *J. Electroanal. Chem.* **1994**, 377 (1–2), 249–259.
- (7) Herron, J. A.; Jiao, J.; Hahn, K.; Peng, G. W.; Adzic, R. R.; Mavrikakis, M. Oxygen Reduction Reaction on Platinum-Terminated “Onion-structured” Alloy Catalysts. *Electrocatalysis* **2012**, 3 (3–4), 192–202.
- (8) Johansson, T. P.; Ulrikkeholm, E. T.; Hernandez-Fernandez, P.; Malacrida, P.; Hansen, H. A.; Bandarenka, A.; Norskov, J. K.; Rossmeisl, J.; Stephens, I. E. L.; Chorkendorff, I. Pt Skin Versus Pt Skeleton Structures of Pt3Sc as Electrocatalysts for Oxygen Reduction. *Top. Catal.* **2014**, 57 (1–4), 245–254.
- (9) Chen, C.; Kang, Y.; Huo, Z.; Zhu, Z.; Huang, W.; Xin, H. L.; Snyder, J. D.; Li, D.; Herron, J. A.; Mavrikakis, M.; Chi, M.; More, K. L.; Li, Y.; Markovic, N. M.; Somorjai, G. A.; Yang, P.; Stamenkovic, V.

- R. Highly crystalline multimetallic nanoframes with three-dimensional electrocatalytic surfaces. *Science (Washington, DC, U. S.)* **2014**, *343* (6177), 1339–43.
- (10) Wang, C.; Stamenkovic, V. R.; Markovic, N. M. Pt terminated PtNi electrocatalysts for the oxygen reduction reaction. *Abstracts of Papers*, 242nd National Meeting of the American Chemical Society, 2011; American Chemical Society: 2011.
- (11) Kuttiyiel, K. A.; Sasaki, K.; Park, G. G.; Vukmirovic, M. B.; Wu, L. J.; Zhu, Y. M.; Chen, J. G. G.; Adzic, R. R. Janus structured Pt-FeNC nanoparticles as a catalyst for the oxygen reduction reaction. *Chem. Commun.* **2017**, *53* (10), 1660–1663.
- (12) Choi, C. H.; Baldizzone, C.; Polymeros, G.; Pizzutilo, E.; Kasian, O.; Schuppert, A. K.; Ranjbar Sahraie, N.; Sougrati, M.-T.; Mayrhofer, K. J. J.; Jaouen, F. Minimizing Operando Demetallation of Fe-N-C Electrocatalysts in Acidic Medium. *ACS Catal.* **2016**, *6* (5), 3136–3146.
- (13) Holby, E. F.; Wu, G.; Zelenay, P.; Taylor, C. D. Structure of Fe-N-x-C Defects in Oxygen Reduction Reaction Catalysts from First-Principles Modeling. *J. Phys. Chem. C* **2014**, *118* (26), 14388–14393.
- (14) Kramm, U. I.; Lefevre, M.; Bogdanoff, P.; Schmeisser, D.; Dodelet, J. P. Analyzing Structural Changes of Fe-N-C Cathode Catalysts in PEM Fuel Cell by Mossbauer Spectroscopy of Complete Membrane Electrode Assemblies. *J. Phys. Chem. Lett.* **2014**, *5* (21), 3750–3756.
- (15) Wu, G.; More, K. L.; Johnston, C. M.; Zelenay, P. High-Performance Electrocatalysts for Oxygen Reduction Derived from Polyaniline, Iron, and Cobalt. *Science (Washington, DC, U. S.)* **2011**, *332* (6028), 443–447.
- (16) Li, J. K.; Ghoshal, S.; Liang, W. T.; Sougrati, M. T.; Jaouen, F.; Halevi, B.; McKinney, S.; McCool, G.; Ma, C. R.; Yuan, X. X.; Ma, Z. F.; Mukerjee, S.; Jia, Q. Y. Structural and mechanistic basis for the high activity of Fe-N-C catalysts toward oxygen reduction. *Energy Environ. Sci.* **2016**, *9* (7), 2418–2432.
- (17) Strasser, P. Catalysts by Platonic design. *Science (Washington, DC, U. S.)* **2015**, *349* (6246), 379–380.
- (18) Gasteiger, H. A.; Markovic, N. M. Just a Dream-or Future Reality? *Science (Washington, DC, U. S.)* **2009**, *324* (5923), 48–49.
- (19) Luo, M.; Guo, S. Strain-controlled electrocatalysis on multimetallic nanomaterials. *Nat. Rev. Mater.* **2017**, *2* (11), 17059.
- (20) Chong, L.; Wen, J.; Kubal, J.; Sen, F. G.; Zou, J.; Greeley, J.; Chan, M.; Barkholtz, H.; Ding, W.; Liu, D.-J. Ultralow-loading platinum-cobalt fuel cell catalysts derived from imidazolate frameworks. *Science (Washington, DC, U. S.)* **2018**, *362* (6420), 1276–1281.
- (21) Ganesan, A.; Narayanasamy, M. Ultra-low loading of platinum in proton exchange membrane-based fuel cells: a brief review. *Materials for Renewable and Sustainable Energy* **2019**, *8* (4), 18.
- (22) Kongkanand, A.; Mathias, M. F. The Priority and Challenge of High-Power Performance of Low-Platinum Proton-Exchange Membrane Fuel Cells. *J. Phys. Chem. Lett.* **2016**, *7* (7), 1127–1137.
- (23) Sharma, R.; Andersen, S. M. Quantification on Degradation Mechanisms of Polymer Electrolyte Membrane Fuel Cell Catalyst Layers during an Accelerated Stress Test. *ACS Catal.* **2018**, *8* (4), 3424–3434.
- (24) Mavrikakis, M.; Nilekar, A. U.; Ford, D. C.; Xu, Y.; Sasaki, K.; Zhang, J.; Vukmirovic, M. B.; Adzic, R. R. Aspects of alloy electrocatalysis. *Abstracts of Papers*, 233rd National Meeting of the American Chemical Society, 2007; American Chemical Society: 2007.
- (25) Kuttiyiel, K. A.; Sasaki, K.; Choi, Y.; Su, D.; Liu, P.; Adzic, R. R. Nitride Stabilized PtNi Core-Shell Nanocatalyst for high Oxygen Reduction Activity. *Nano Lett.* **2012**, *12* (12), 6266–6271.
- (26) Kuttiyiel, K. A.; Choi, Y.; Hwang, S.-M.; Park, G.-G.; Yang, T.-H.; Su, D.; Sasaki, K.; Liu, P.; Adzic, R. R. Enhancement of the oxygen reduction on nitride stabilized Pt-M (M = Fe, Co, and Ni) core-shell nanoparticle electrocatalysts. *Nano Energy* **2015**, *13*, 442–449.
- (27) Fan, H. B.; Yuen, M. M. Material properties of the cross-linked epoxy resin compound predicted by molecular dynamics simulation. *Polymer* **2007**, *48* (7), 2174–2178.
- (28) Sun, H.; Jin, Z.; Yang, C.; Akkermans, R. L.; Robertson, S. H.; Spenley, N. A.; Miller, S.; Todd, S. M. COMPASS II: extended coverage for polymer and drug-like molecule databases. *J. Mol. Model.* **2016**, *22* (2), 47.
- (29) Sun, H. COMPASS: An ab Initio Force-Field Optimized for Condensed-Phase Applications Overview with Details on Alkane and Benzene Compounds. *J. Phys. Chem. B* **1998**, *102*, 7338–7364.
- (30) Mansour, A. N.; Cook, J. W.; Sayers, D. E. Quantitative technique for the determination of the number of unoccupied d-electron states in a platinum catalyst using the L_{2,3} x-ray absorption edge spectra. *J. Phys. Chem.* **1984**, *88* (11), 2330–2334.
- (31) Lytle, F. W. Determination of d-band occupancy in pure metals and supported catalysts by measurement of the LIII X-ray absorption threshold. *J. Catal.* **1976**, *43* (1), 376–379.
- (32) Lytle, F. W.; Wei, P. S. P.; Gregor, R. B.; Via, G. H.; Sinfelt, J. H. Effect of chemical environment on magnitude of x-ray absorption resonance at LIII edges. Studies on metallic elements, compounds, and catalysts. *J. Chem. Phys.* **1979**, *70* (11), 4849–4855.
- (33) Hammer, B.; Nørskov, J. K. Theoretical surface science and catalysis—calculations and concepts. *Adv. Catal.* **2000**, *45*, 71–129.
- (34) Zhang, J.; Vukmirovic, M. B.; Xu, Y.; Mavrikakis, M.; Adzic, R. R. Controlling the Catalytic Activity of Platinum-Monolayer Electrocatalysts for Oxygen Reduction with Different Substrates. *Angew. Chem., Int. Ed.* **2005**, *44* (14), 2132–2135.